Positron Range Effects on the Spatial Resolution of RPC-PET

A. Blanco

***Abstract*– This work studies, by simulation, the influence of the positron range into the sub-millimeter spatial resolution of an experimental prototype of Resistive Plate Chamber (RPC) to be applied to small animal Positron Emission Tomography (PET) – a system able to see directly a reasonable region of the positron distribution tail .**

Employing a Monte Carlo simulation code (Geant4) the positron range distributions, for eight radioisotopes of interest to PET: ^{22}Na, ^{18}F, ^{11}C, ^{13}N, ^{15}O, ^{68}Ga and ^{82}Rb was modeled.

It was found that, owing to the non-Gaussian nature of the positron range distribution, which partially remains in the Point Spread Function (*PSF*) of the system, a direct image spatial resolution enhancement is achieved. It was experimentally verified that this enhancement is around 10% FWHM for a ^{22}Na point-like source achieving an image spatial resolution of 470 μm FWHM.

The simulated positron distributions compare reasonably well with the experimental measurements from the RPC-PET prototype and with values reported by other authors.

I. Introduction

POSITRON EMISSION TOMOGRAPHY (PET) is one of the in vivo imaging modalities largely developed in the last decades. Its strength resides in the ability to accurately measure the amount of radioactive tracer accumulation in organs, merging the best combination of sensitivity and spatial resolution. In particular, small animal PET has driven significant advances in high spatial resolution PET systems [1, 2 and 3]. These instruments are approaching the fundamental limits on spatial resolution imposed by the physics of positron annihilation, i.e. positron range and annihilation photon non-collinearity. The annihilation photon non-collinearity is originated by the conservation of the residual momentum of the electron-positron system just prior to annihilation at the end of the positron's path. As a result, the angular separation between the two photons emitted deviates from 180º. This effect is well characterized [4 and 5] and a simple way to minimize it is by reducing the photons path length, which is achieved in practice by minimizing the detector ring diameter (see [6]). The positron range effect is originated by the displacement of the annihilation site from the point of positron emission. The only know way to reduce this effect is using a strong magnetic field, an attractive approach [7, 8 and 9], since the PET scanner can be potentially merged with a Magnetic Resonance Imaging (MRI) scanner. It is the largest contribution, at least for small animal PET systems and high energy radiotracers, and probably the least understood.

The RPC-PET, previously introduced [10 and 11], is a prototype of PET system based on timing Resistive Plate Chamber (tRPC) Technology [12]. The prototype is composed of two detecting elements, see Figure 1, built from sixteen counters each, able to measure the photon interaction point in two dimensions: the tangential coordinate and the Depth of Interaction (DOI). By imaging point-like ^{22}Na positron sources located in the transaxial plane at different positions along the tangential direction, a homogeneous image spatial resolution of 0.3 mm FWHM and 0.8 mm FWTM was obtained after reconstruction by an ML-EM type algorithm [13], demonstrating the parallax-free imaging capability of the system [6]. How ever, the resolution is largely influenced by the annihilation photon non-collinearity and the positron range effects, which dominate the Point Spread Function (*PSF)* tails.

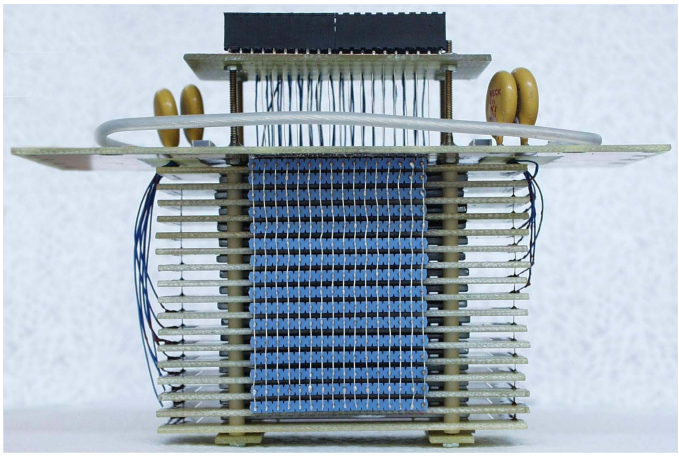

Fig.1. Detecting element built with 17 identical stacked plates, which define 16 independent sensitive gas gaps, being able to measure the photon interaction point in two dimensions: the tangential dimension and the DOI.

With a view to understanding the effects of the positron range into the image spatial resolution of the RPC-PET prototype, the positron distribution was simulated using the Geant4 toolkit. The results are compared with experimental measurements and values from other authors.

Manuscript received November 4, 2006. This work was supported by Fundação para a Ciência e Tecnologia and FEDER under contracts POCI/FP/63411/2005 and POCI/SAU-OBS/61642/2004 and by "Instituto de Investigação Interdisciplinar da Universidade de Coimbra".

A. Blanco is with LIP, Laboratório de Instrumentação e Física Experimental de Partículas, Coimbra 3004-516, Portugal (e-mail: alberto@coimbra.lip.pt).

II. METHODS

A. The Monte Carlo Simulation.

The Geant4.05.02 toolkit [14] was used to simulate the transport in water of positrons emitted by different radioisotopes of interest to PET: ^{22}Na, ^{18}F, ^{11}C, ^{13}N, ^{15}O, ^{68}Ga and ^{82}Rb. For each radioisotope the simulation was run three times using standard Geant4, the low energy (LE) extension and the PENELOPE (PE) physics extension.

An isotropic point-like positron source was situated at the origin of coordinates centered in a sphere of water with an infinite radius. The characteristic β^+ energy spectrum for the different radioisotopes (see Figure 2) was generated using the analytical expression taken from [15]:

$$N(E)dE = g(E)F\sqrt{E^2-1}E(E_{\max}-E)^2 dE$$

where *N(E)* is the number of decays at energy *E*, *g(E)* is a coupling constant, *F* is the Fermi function and E_{max} is the maximum (end point) energy of the β^+ particle.

The end point coordinate of each event was recorded, representing the 3D annihilation Point Spread Function (*aPSF*), i.e. the *PSF* only due to the positron range contribution.

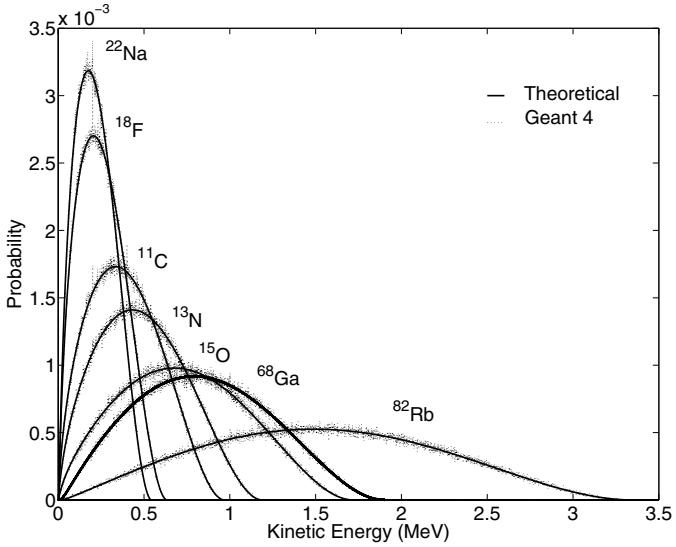

Fig.2. Theoretical positron kinetic energy spectra and Geant4 output for different radionuclides.

Two 1D distributions were calculated for each 3D *aPSF*: the projection onto one dimension, the z direction

$$aPSFs(z) = \int_{-\infty}^{\infty} dy \int_{-\infty}^{\infty} aPSF(x,y,z)dx$$

which is the distribution that contributes directly to the sinogram *PSF* (*PSFs*) and the 1D profile, at the maximum, of the projection onto the xz plane, perpendicular to the axis of the scanner

$$aPSFi(z) = \int_{-X_m+\Delta x/2}^{X_m+\Delta x/2} dx \int_{-\infty}^{\infty} aPSF(x,y,z)dy$$

where X_m is the location of the maximum of the projected distribution onto the xz plane and Δx is a the sampling interval on x. This *aPSFi* is the relevant distribution contributing to the image *PSF* (*PSFi*) and therefore to the image spatial resolution.

These 1D distributions where characterized by a fit to the sum of two exponential functions [16] was performed

$$P(z) = Ce^{-k_1|z|} + (1-C)e^{-k_2|z|} \quad (1)$$

where C, k_1 and k_2 are the fitted parameters.

B. Experimental measurements

By using the RPC-PET prototype described in the introduction, the experimental *PSFs* and *PSFi* (obtained through the filtered back projection algorithm) were measured using a point-like ^{22}Na positron source, centered in the Field of View (*FOV*). Both *PSF* were fitted with a function

$$R(z) = C_2(N(z) \otimes P(z) \otimes D(z) \otimes S(z)) + (1- C_2)SC(z) \quad (2)$$

which convolutes all instrumental and physical contributions: annihilation photon non-collinearity *N(z)*, positron range *P(z)*, detector response *D(z)*, source size *S(z)* and scatter background *SC(z)*, as described in [10]. This fit allows us to retrieve some of the system parameters (FWHM, FWTM) as well as the k_2 parameter (see eq. 1), which represents the positron range distribution tails, enabling a direct comparison with the simulation and with other authors.

III. RESULTS

The results obtained with the three physics models used in the simulation are very similar. This can be seen in figure 6 where the k_2 parameter is compared for the three models as a function of the E_{max} energy of each radioisotope. The differences in the *C*, k_1 and k_2 parameters are at a level of 2%.

It was found that the *aPSFs* and the *aPSFi* distributions have different shapes and therefore they contribute in different ways to the sinogram and to the image. Figure 3a shows both distributions for a ^{18}F point source simulated with Geant4 LE. The *aPSFi* exhibits a narrower and sharper shape compared with the *aPSFs*. This is a particular characteristic of the shape of the positron range distribution and it is not applicable, e. g. to a Gaussian distribution, which shows the same distributions for the *aPSFs* and *aPSFi,* see figure 3b.

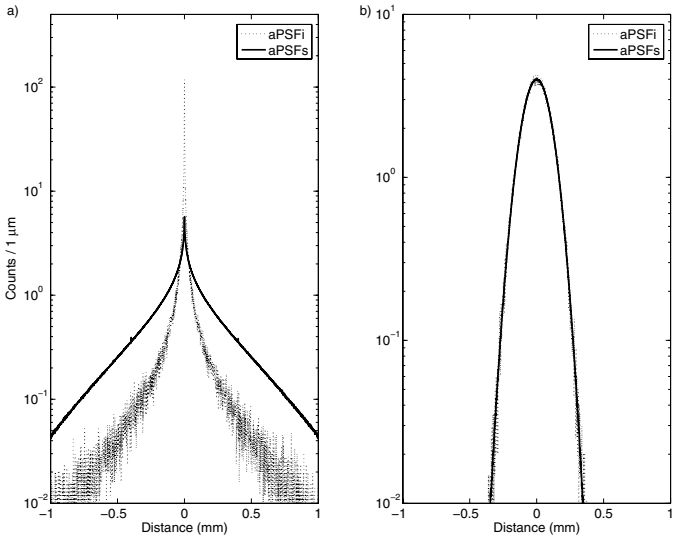

Fig.3. *aPSFs* and *aPSFi* distributions from a) a point-like ^{18}F source (simulated with Geant4 LE) and b) Gaussian distribution.

As a consequence, when the *PSF* preserves some information of the original *aPSF*, a direct image spatial resolution enhancement is obtained with respect to the corresponding sinogram, in contrast with systems with Gaussian *PSF*. This is experimentally observed on the RPC-PET prototype as can be seen in figure 4, where the measured *PSFs* and *PSFi*, for the ^{22}Na source, were fitted to the function *R(z)* yielding 520 µm and 470 µm FWHM, respectively, and 1550 µm and 1120 µm FWTM. This represents a gain in the image spatial resolution of ~ 10% at FWHM and ~ 27% at FWTM.

The best fit parameters of equation 1 to the simulated *aPSFs* and *aPSFi* (using a 10 µm bin) for the eight different radioisotopes are shown in table I.

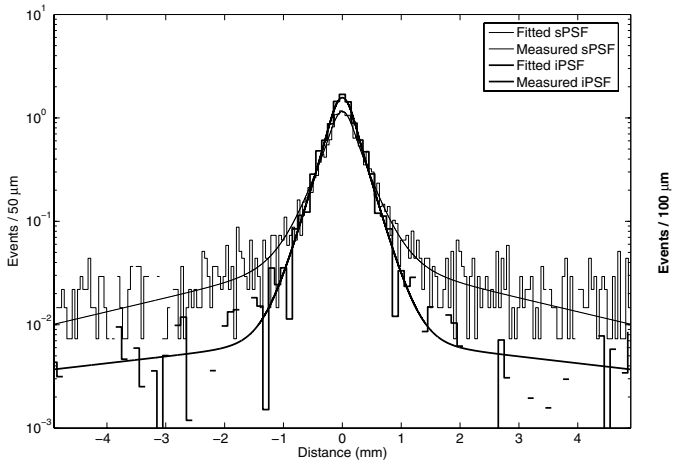

Fig.4. Measured and fitted *PSFs* and *PSFi,* for a ^{22}Na source, shown an image enhancement of ~ 10% at FWHM.

The simulated k_2 parameter for the ^{22}Na can be compared with the measured values taken from the fit of equation 2 to the measured *PSFs* and *PSFi.* In order to perform a correct comparison, the binning used in the simulated distributions must be equal to the binning used in the measured distributions. The values obtained from the simulation for k_2 are 4.29 mm^{-1} and 5.2 mm^{-1} over *aPSFs* and *aPSFi* and the measured ones are 3.75 mm^{-1} and 4.45 mm^{-1} over *PSFs* and *PSFi* respectively. The difference between the measured and simulated values, at a level of ~ 12%, could be originated by the sensitivity of the fit, to the measure *PSF* with the amount of scatter shown.

A comparison with the *aPSF* results from Derenzo [16] and Levin [17] is also possible. Figure 5 shows the measured *aPSF* from Derenzo a) and Levin b) compared with the Geant4 LE simulation. The appropriate binning was used in each case to enable a direct comparison.

TABLE I
BEST FIT PARAMETERS OF EQUATION 1 FOR aPSFs AND aPSFs

		aPSFs			*aPSFi*		
Isotope	E_{max} (MeV)	C	K_1 (mm^{-1})	K_2 (mm^{-1})	C	K_1 (mm^{-1})	K_2 (mm^{-1})
^{22}Na	0.545	0.509	21.11	4.27	0.894	30.93	5.52
^{18}F	0.634	0.497	17.11	3.38	0.893	24.01	4.30
^{11}C	0.960	0.447	9.83	1.78	0.876	12.77	2.26
^{13}N	1.199	0.408	7.80	1.31	0.825	10.40	1.69
^{15}O	1.735	0.346	5.48	0.77	0.870	7.37	1.02
^{68}Ga	1.885	0.255	5.39	0.65	0.830	6.62	0.88
^{82}Rb	3.264	0.174	4.33	0.30	0.798	4.05	0.43

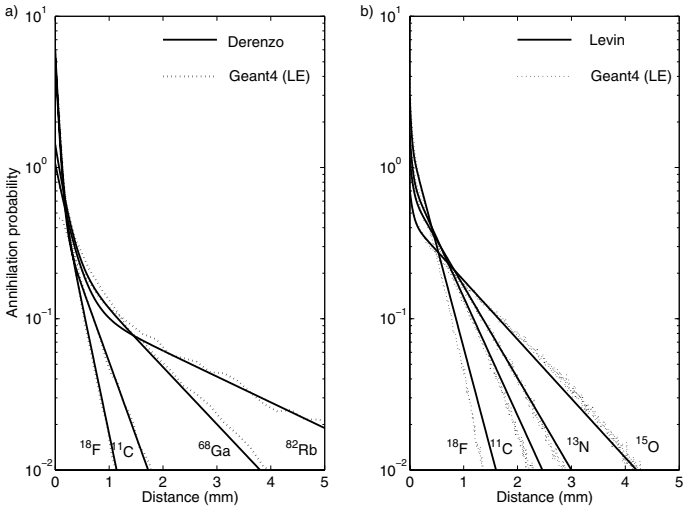

Fig.5. *aPSF,* reported by Derenzo a) and Levin b) compared with the Geant4 LE simulation for different radioisotopes.

The agreement between Geant4 and the results from Derenzo and Levin are quite good. It should be noted that the Derenzo measurements correspond to the *aPSFi* whereas the results reported by Levin correspond to the *aPSFs*. Values for k_2 parameter are also shown in figure 6 as a function of the E_{max} energy for the three different physics approaches and the values reported by Derenzo a) and Levin b).

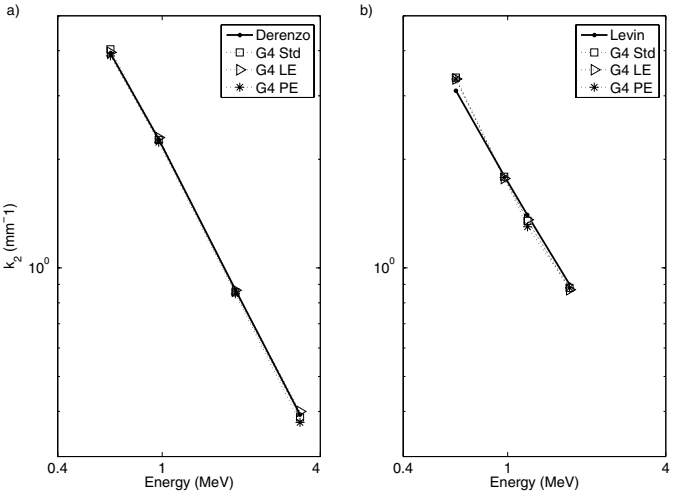

Fig.6. Comparison of the k_2 parameter from the three used simulation models and measured data from Derenzo a) (*PSFi*) and simulated data from Levin b) (*PSFs*) as a function of the E_{max} energy of each radioisotope.

I. Conclusions

As the RPC-PET technology is able to see partially the positron range distribution on the *PSF*, its effects on the spatial resolution have been studied by simulation.

It was found, that owing to the non-Gaussian nature of the positron range distribution, which partially remains in the *PSF* of the system, the image spatial resolution is enhanced with respect to the corresponding sinogram. This enhancement is approximately 10% FWHM and 27% FWTM for a ^{22}Na point-like positron source. The image spatial resolution achieved is 470 μm FWHM and 1120 μm FWTM.

The positron range distributions for eight positron emitters of interest to PET, ^{22}Na, ^{18}F, ^{11}C, ^{13}N, ^{15}O, ^{68}Ga and ^{82}Rb, were simulated with the Geant4 toolkit, using three physics models showing to be in close agreement, at a level of 2%.

The simulations were also compared with experimental measurements from the RPC-PET prototype, which is able to see directly a reasonable region of the positron distribution tail, and with values reported by other authors, showing a good agreement.

Acknowledgment

The author gratefully acknowledges the special contribution from P. Fonte and the collaboration of N. Carolino, L. Lopes and A. Pereira by their support as well as for many useful discussions.

References

[1] A.P. Jeavons, R.A. Chandler, C.A.R. Dettmar, "A 3D HIDAC-PET Camera with Sub-millimetre Resolution for Imaging Small Animals", *IEEE Trans. Nucl. Sci., vol. 46, No. 3, June 1999, 468-473.*

[2] Yuan-Chuan Tai et al., "MicroPET II: design, development and initial performance of an improved MicroPET scanner for small-animal imaging", *Phys. Med. Biol. 48 (2003) 1519-1537.*

[3] A. del Guerra, G. Di Domenico, M. Scandola, G. Zavattini, "YAP-PET: first results of a small animal Positron Emission Tomograph based on YAP:Ce finger crystals", *IEEE Trans. Nucl. Sci., vol 45, No. 6 December 1998, 3105-3108.*

[4] DeBenedetti S, Cowan C. E., Konneker W. R. and Primakoff H., "On angular distribution of two-photon annihilation radiation", *Phys. Rev. 77 (1950) 205-12*

[5] W. W. Moses, S. E. Derenzo, "Empirical observation of resolution degradation in positron emission tomographs utilizing block detectors", *J. Nucl. Med 34 (1993) 101.*

[6] A. Blanco et al, "Very high position resolution gamma imaging with resistive plate chambers", *Nucl. Instr. And Meth. A, in Press.*

[7] Raymond R. Raylman, Bruce E. Hammer and Nelson L. Christensen, "Combined MRI-PET scanner: A Monte Carlo evaluation of the improvements in PET resolution due to the effects of a static homogenous magnetic field", *IEEE Trans. Nucl. Sci., vol 43 No 4, August 1996.*

[8] Andreas Wirrwar et al, "4.5 Tesla Magnetic Field Reduces Range of high-Energy Positrons—Potential Implication for Positron Emission Tomography", *IEEE Trans. Nucl. Sci., vol 44 N0 2, April 1997.*

[9] A. Blanco et al, "Spatial resolution on a small animal RPC-PET prototype operating under magnetic field", *Nuclear Physics B - Proceedings Supplements Vol 158, 157-160, August 2006*

[10] A. Blanco et al., "RPC-PET: A new very high resolution PET technology", to be published in *IEEE Trans. Nucl. Sci., vol 53, No. 5, October 2006.*

[11] A. Blanco, et al., "An RPC-PET prototype with high spatial resolution", *Nucl. Instr. and Meth. A 533 (2004) 139-143*

[12] P. Fonte, A. Smirnitski, M.C.S. Willians, "A new high resolution TOF technology*", Nucl. Instr. And Meth. A, 443 (2000) 201-204.*

[13] L. Fazendeiro, et al., "EM Reconstruction algorithm with resolution modeling applied to an RPC-PET prototype", *proceedings of IEEE Medical Image Conference 2004, M2-177.*

[14] Geant4 http://wwwasd.web.cern.ch/wwwasd/geant4/geant4.html

[15] Evans, Robley D. "The atomic nucleus", New York McGraw-Hill, 1972

[16] Stephen E. Derenzo, "Mathematical removal of positron range blurring in high resolution tomography*", IEEE Trans. Nucl. Sci., vol 33, No. 1, February 1986, 565-569.*

[17] Craig S. Levin, Edward J. Hoffman, "Calculation of positron ranges and its effect on the fundamental limit of the positron emission tomography system spatial resolution", *Phys. Med. Biol. 44 (1999) 781-799.*